Chemical and Process Engineering: New Frontiers, 2025, 46(4), e109
DOI: 10.24425/cpe.2025.155547

The effect of sintering temperature on the microstructure and selected properties of composites on Fe with the addition of SiC produced with spark plasma sintering

Małgorzata Perek-Nowak[1], Teresa Bajor[2], Monika Górska[2*], Kinga Ostafińska[1]

[1] AGH University of Krakow, Faculty of Non-Ferrous Metals, 30 Mickiewicza Ave, 30-059 Krakow, Poland
[2] Czestochowa University of Technology, Faculty of Production Engineering and Materials Technology, Armii Krajowej 19, 42-201 Czestochowa, Poland

*** Corresponding author, e-mail:**
monika.gorska@pcz.pl

Presented at
MEMSEP & PERMEA 2025
15th International Conference
on Membrane and Separation
Processes & 10th Membrane
Conference of Visegrad Countries
24–26 June, 2025, Chorzów, Poland.
Guest Editor: Maciej Szwast

Article info:
Received: 16 June 2025
Revised: 25 August 2025
Accepted: 17 September 2025

Abstract
The article presents the microstructure observations and selected mechanical properties of composites with Fe or Distaloy matrix and the addition of the SiC reinforcing phase. Composites with the content of 2.5, 5, 7.5, 10 and 12.5% SiC were prepared. The samples were prepared at the Spark Plasma Sintering (SPS) 10-4 device applying a sintering temperature of 950 °C and 1000 °C. Depending on the SiC content, composites with a density of 93–98% of pure iron were obtained. The results showed differences in the microstructure of composites reinforced with SiC particles in the form of complex phases appearing. The effect of the amount of SiC addition on the hardness of the materials studied was also analyzed.

Keywords
Spark Plasma Sintering (SPS), Fe–SiC, Distaloy, sintering powder, microhardness

1. INTRODUCTION

Powder metallurgy is an attractive technology from the point of view of producing metal alloys due to its many advantages. This includes obtaining a material with a homogeneous microstructure and controlled distribution of precipitates, which give the alloys excellent isotropic properties (Chen et al., 2021; Li et al., 2020). Initially, the powder densification and sintering focused on the high-speed steel with the addition of hard ceramics such as titanium carbide TiC (Jarząbek et al., 2015; Li et al., 2020; Sui et al.; 2018), vanadium carbide VC (Huang et al., 2016; Zhang et al., 2019), manganese sulfide MnS (Zalisz et al., 2005), niobium carbide NbC (Zapata et al., 1998), alumina Al_2O_3 and titanium nitride TiN (Mutuchamy et al., 2018). However, the use of this method to obtain various alloys is becoming more and more widespread, an example of which is research on obtaining composites based on Al (Bedir, 2007; Leszczyńska-Madej et al., 2019; Madej et.al., 2022), Cu (Eze et al., 2022; Sulima et al., 2024) or Ti (Zhang et al., 2022).

Metal Matrix Composites (MMCs) are of great interest due to the wide possibilities of controlling the level of mechanical properties. The Spark Plasma Sintering (SPS) methodology allows for their modification by means of the size of the particles used, particle morphology, particle composition or distribution of various reinforcing phases. There are many publications in the world literature describing the technologies for obtaining many materials using this method. Marnier et al. (2014), showed that SPS technology can be used to produce 316L steel in order to achieve the appropriate microstructure. Shashanka (2019), describes the5 use of the SPS method for consolidation of ground stainless steel powders at a temperature of 1050 °C. It has been shown that the SPS technique increases the density, hardness and wear resistance of stainless steels.

Muthuchamy et al. (2018) presented the effect of alloying additions such as copper, carbon and molybdenum with carbonyl iron powder on the densification behavior, microstructure evolution and mechanical properties of compacts sintered with the SPS method. It was shown that after sintering at a temperature of 1120 °C it was possible to obtain a material with a density of 97%, good hardness (97 HRB) and a beneficial effect of molybdenum addition on grain refinement. MMCs are widely used in many industries, including: metallurgical, mining, aviation, energy, automotive and other fields because they are characterized by better strength and plasticity, as well as high strength, hardness and wear resistance (Chen et al., 2021; Jarząbek et al., 2015; Li et al., 2020; Sui et al., 2018; Wang et al., 2021).

The main objective of this work was to determine influence of chemical composition and the manufacturing parameters on microstructure and properties of Fe–SiC and Distaloy-SiC composites produced using powder metallurgy technology.

2. MATERIALS, EQUIPMENT AND RESEARCH METHODOLOGY

Two types of mixtures were used to produce the composites. The first was based on Fe and the other was based on Distaloy SA prealloyed powder with the chemical composition shown in Table 1. The composite mixtures were enriched with SiC powder with granulation below 10 µm with different share of the reinforcing phase (Table 2).

Table 1. Chemical composition of the Distaloy SA alloy.

Material/% wag	Fe	Ni	Cu	Mo
Distaloy SA	96.25	1.75	1.5	0.5

Before the sintering process, the components were mixed in a Turbula T2F mixer (WAB, Switzerland) for about 1 hour.

The sintering process was carried out using the SPS 10-4 device (Thermal Technology LLC) owned by the Faculty of Production Engineering and Materials Technology, Czestochowa University of Technology, Poland (Fig. 1).

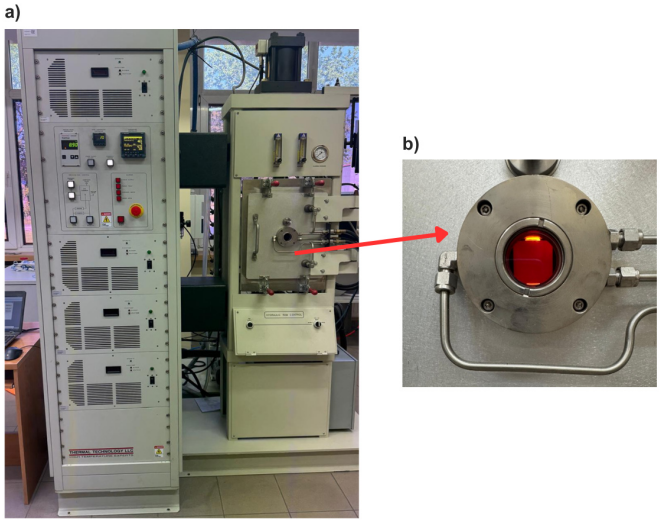

Figure 1. View of a) the SPS 10-4 device and b) sample system during the process.

Sintering was performed using tools made of 2333 (Mersen) graphite. The sintering process was carried out in vacuum. The size of the sintered samples was 20 mm in diameter and about 10 mm in height.

After the sintering process, the density of the obtained sinters was determined in accordance with the PN-EN ISO 2738:2001 standard.

Microscopic observations of the structures after the sintering process were carried out at Hitachi S-3400N scanning electron microscope (SEM), equipped with a tungsten gun with thermoemission and a special attachment for EDS analysis by Thermo Noran.

Hardness measurements were performed using the Vickers method.

3. RESEARCH RESULTS

Before the sintering process, powders were examined using SEM. Powders of pure iron, Distaloy SA and silicon carbide were analyzed at magnifications from 200 to 10.000 times in SE contrast (Figures 2–4).

Iron powder and Distaloy SA iron show similar features. Powder particles in both cases are characterized by a globular shape. However, in the case of Distaloy SA iron, irregular particles can also be observed in some places, which results from the chemical composition of this powder. In turn, silicon carbide powder takes the form of polyhedral and irregular particles with sharp edges and high density. Besides, SiC powder is much finer with average size of 2 µm.

In order to determine the sintering temperature, preliminary tests were carried out for a mixture of powders prepared independently. Based on preliminary tests, the parameters of the sintering process of the mixture were determined: temperature and sintering time of 950 °C and 1000 °C and 10 min in vacuum. A pressing pressure of 50 MPa and a constant heating rate of 100 °C/min were used. The pulse duration was 15 ms, the duration of the pause between pulses was 20% of the pulse duration. Preliminary tests showed that when the sintering temperature reached 1000 °C (Fig. 5), a plateau effect could be observed in the densification curves, indicating full densification of the sintered powder. At lower sintering temperatures, the plateau effect was not visible throughout the sintering process.

After consolidation and sintering, sinters with a diameter of Ø20 and a height of 10 mm were obtained. Density measurements were performed. The results of density measurements of the samples after the sintering process are presented in Table 3.

Table 2. Chemical composition of composite mixtures, %.

Composite mixtures	Fe–SiC					Distaloy SA-SiC				
Admixture content SiC [%]	2.5	5	7.5	10	12.5	2.5	5	7.5	10	12.5

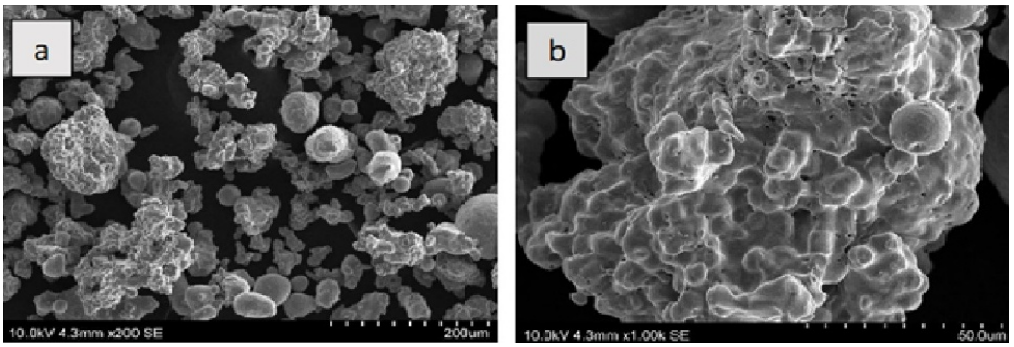

Figure 2. Morphology of iron powder in SE contrasts at magnification of a) 200x and b) 1000x.

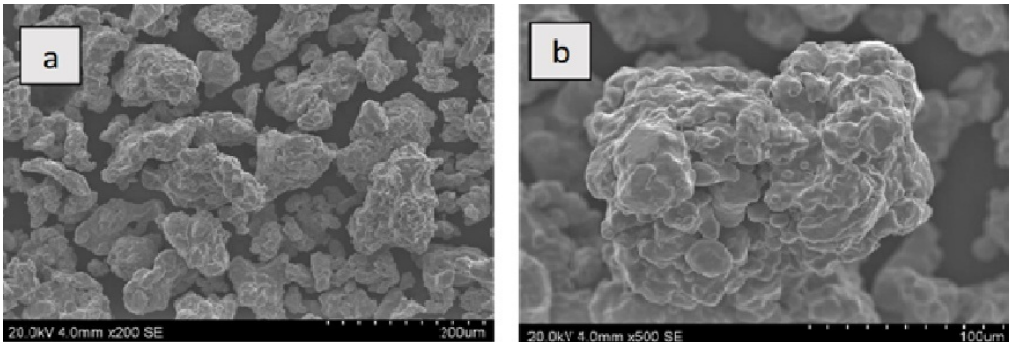

Figure 3. Morphology of Distaloy SA prealloyed iron powder in SE contrast at magnification of a) 200x and b) 500x.

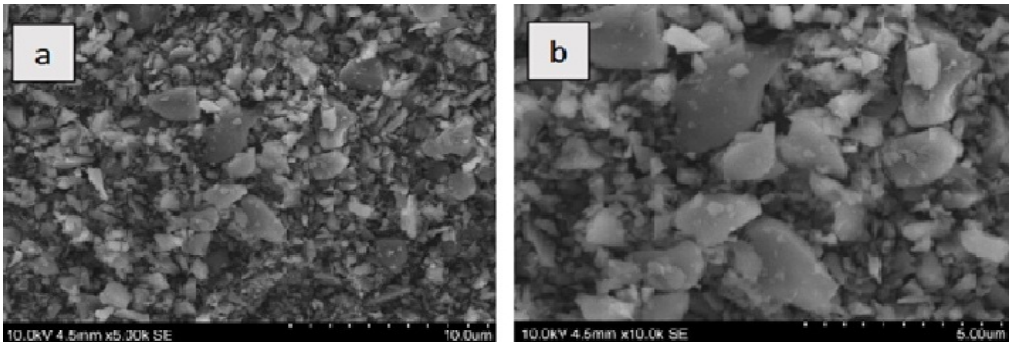

Figure 4. Morphology of silicon carbide powder in SE contrast at magnification of a) 5000x and b) 10000x.

Table 3. Results of density measurements of samples after the sintering process at temperature of 1000 °C.

Theoretical density	Composite composition	Density [g/cm^3]	% of theoretical density
Fe 7.875 g/cm^3	Fe – 2.5% SiC	7.660	97.3
	Fe – 5% SiC	7.640	97.0
	Fe – 7.5% SiC	7.615	96.7
	Fe – 10% SiC	7.519	95.5
	Fe – 12.5% SiC	7.329	93.1
Distaloy SA 7.93 g/cm^3	Distaloy – 2.5% SiC	7.606	95.9
	Distaloy – 5% SiC	7.603	95.9
	Distaloy – 7.5% SiC	7.549	95.2
	Distaloy – 10% SiC	7.513	94.7
	Distaloy – 12.5% SiC	7.339	92.5

The data presented in Table 3 show that the increase in SiC content significantly affects the change in the density of the samples. In the case of Fe powders, the addition of SiC in the amount of 2.5, 5 and 7.5 causes a decrease in density to a level above 95%, as shown in Figure 6.

In order to conduct a more complete analysis of the obtained composites a microstructure analysis was performed, selected images of materials on the iron matrix and Distaloy SA iron with a variable content of SiC addition were compared. The obtained images of microstructures are shown in Figures 7–10. The photos were taken at different magnifications on a scanning microscope and BSE contrast.

Silicon carbide is revealed in the structures of both types of materials in the form of black inclusions at the grain boundaries which create numerous agglomerates depending on the amount of SiC phase addition. Based on the observations carried out, it can be seen that their distribution in the matrix is quite uniform. The highest share of the SiC phase was observed in the case of samples with its maximum content in the matrix. Comparing the tested base materials, a larger number of silicon carbide clusters was observed in the case of composites based on pure iron. The lighter, gray areas constitute the matrix of the composites, which is rich in iron and has a ferritic character – typical for this element during the sintering process. The presence of pearlite was also observed in the microstructure of the tested materials. Pearlite structures are formed during sintering when some silicon carbide particles disintegrate. It can be suspected that pearlite is formed only in places where carbon concentration increases to an appropriate level during diffusion. Both silicon and carbon atoms can diffuse into iron particles, and the

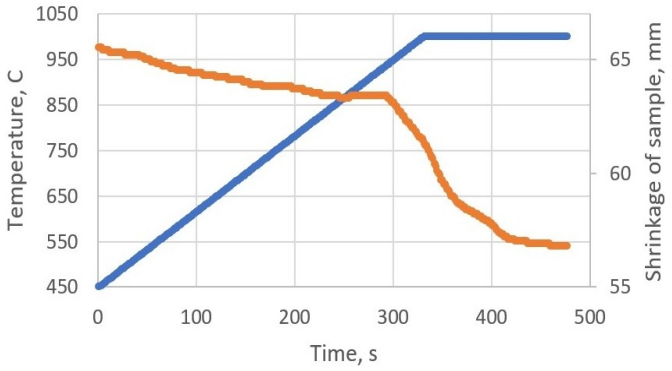

Figure 5. Dependence of temperature change and sample shrinkage during sintering using the SPS method for Fe – 12.5% SiC.

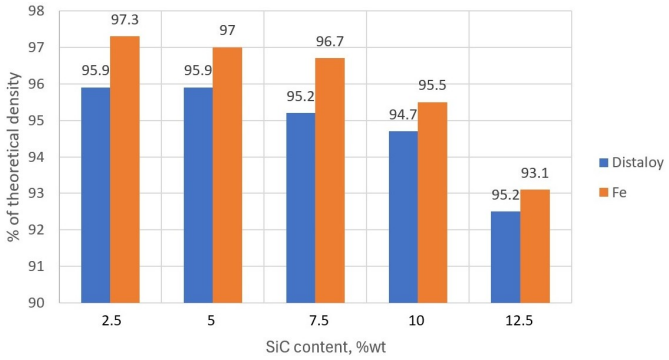

Figure 6. Level (%) of theoretical density depending on SiC content for Fe and Distaloy based composites.

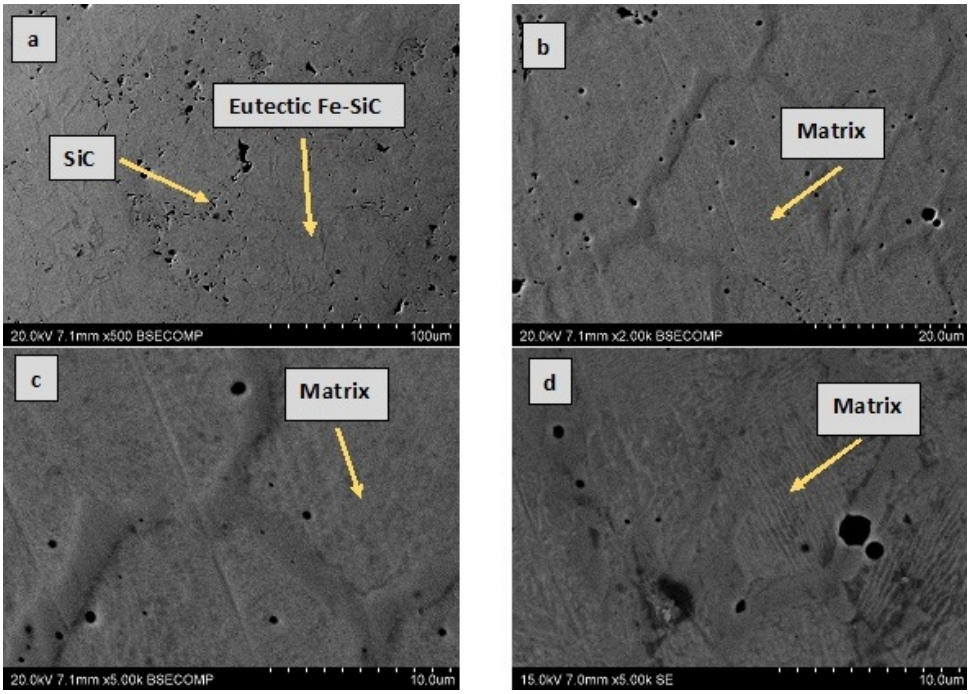

Figure 7. Microstructure image of Fe – 2.5% SiC sinter in BSE contrast at magnification of a) 500x, b) 2000x, c) 5000x and d) 5000x.

decomposition of the Fe–C solid solution results in the formation of alternating layers of ferrite and cementite. This state is confirmed by the microstructure image taken for the sample with the composition Fe – 12.5% SiC (Figure 8).

In the microstructure of the Fe-based samples, one can see the formation of eutectic, which is mostly located at the grain boundaries. It can be seen that in the materials based on pure iron, the amount of eutectic decreases with the increase in the addition of silicon carbide, which results in an increased tendency to form porosity in the material. The eutectic in the case of sinters made from Distaloy SA powders is more developed, as indicated in Figure 6b, than that for pure iron powder. Similarly to the previous case, it is formed in the vicinity of the grain boundaries and its amount increases with the increasing content of silicon carbide in the composite. Consequently, the sample with the largest amount of silicon carbide shows the characteristics of the material with the lowest porosity.

The next stage of the research was to conduct a detailed analysis of the resulting compounds. Analysis of Fe – 12.5% SiC (Figure 11a) for points 1–2 marked in the images allow for the presence of an eutectic phase, which is formed in the vicinity of grain boundaries. In points 3–5, a matrix area enriched with small additions of silicon and carbon is visible (Table 4). The EDS analysis conducted for the composite

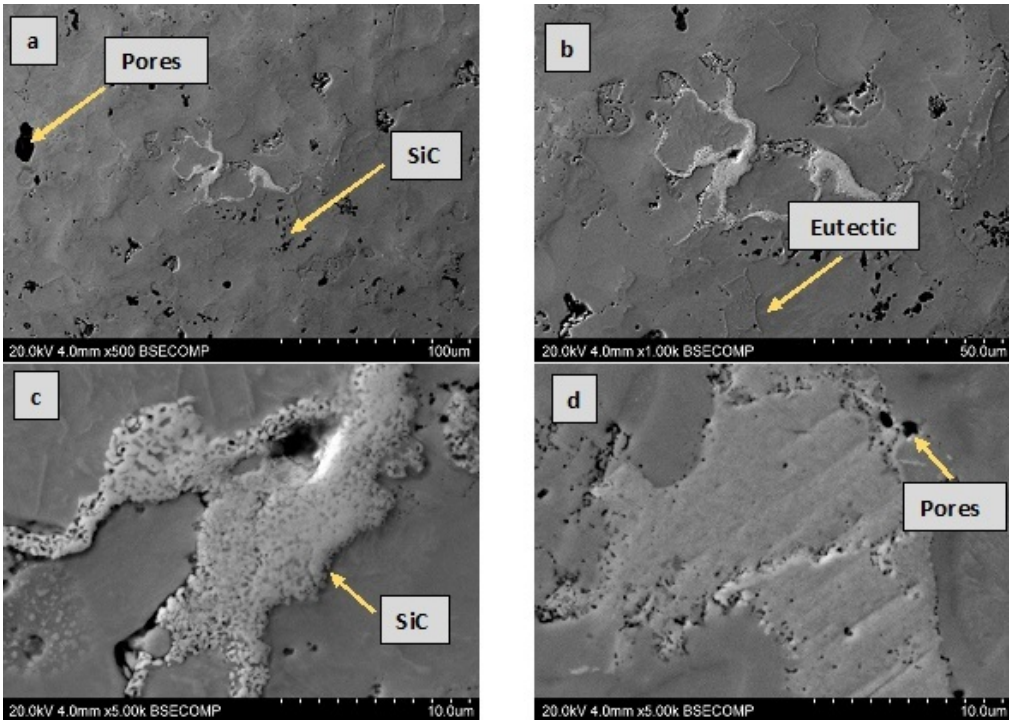

Figure 8. Microstructure image of Distaloy SA – 2.5% SiC sinter in BSE contrast at magnification of a) 500x, b) 1000x, c) 5000x and d) 5000x.

Table 4. EDS analysis results for the material: Fe – 12.5% SiC and Distaloy SA – 12.5% SiC.

Name of the mixture	Point	C-K	Si-K	Fe-K	Ni-K	Cu-K	Mo-L
Fe – 12.5% SiC	1	11.44	4.41	84.15	–	–	–
	2	18.85	12.35	68.82	–	–	–
	3	1.69	3.29	95.02	–	–	–
	4	2.38	4.39	93.23	–	–	–
	5	2.79	3.3	93.91	–	–	–
Distaloy – 12.5% SiC	1	4.99	5.95	47.54	1.84	–	39.69
	2	2.32	7.5	86.25	3.93	–	–
	3	2.46	7.09	87.50	2.95	–	–
	4	2.56	5.25	89.52	–	2.67	–
	5	2.25	1.98	95.77	–	–	–
	6	5.57	0.98	93.46	–	–	–

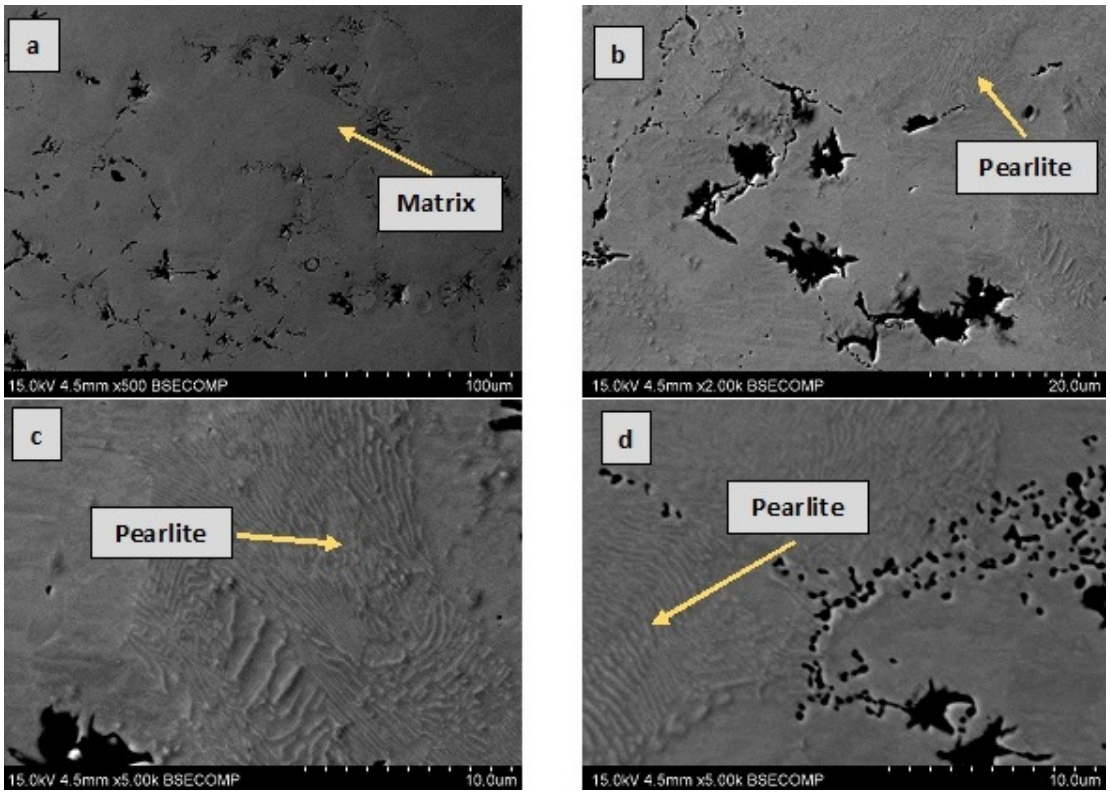

Figure 9. Microstructure image of Fe – 12.5% SiC sinter in BSE contrast at magnification of a) 500x, b) 2000x, c) 5000x and d) 5000x.

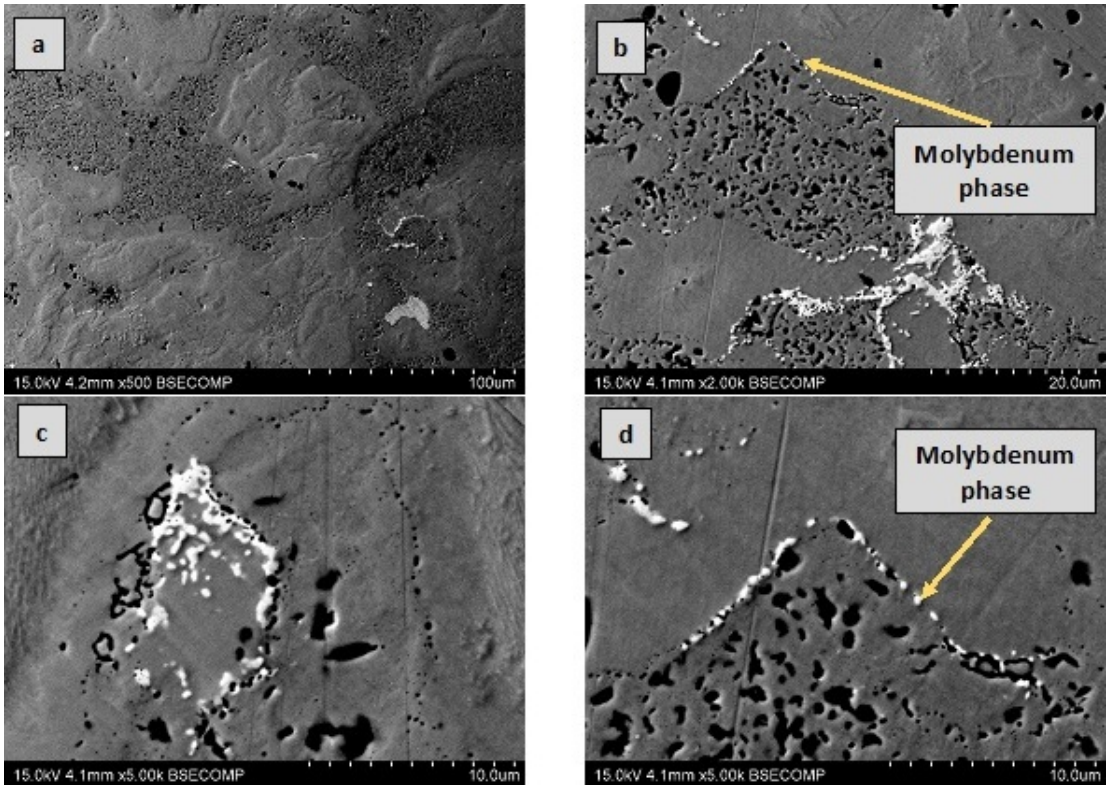

Figure 10. Microstructure image of Distaloy – 12.5% SiC sinter in BSE contrast at magnification of a) 500x, b) 2000x, c) 5000x and d) 5000x.

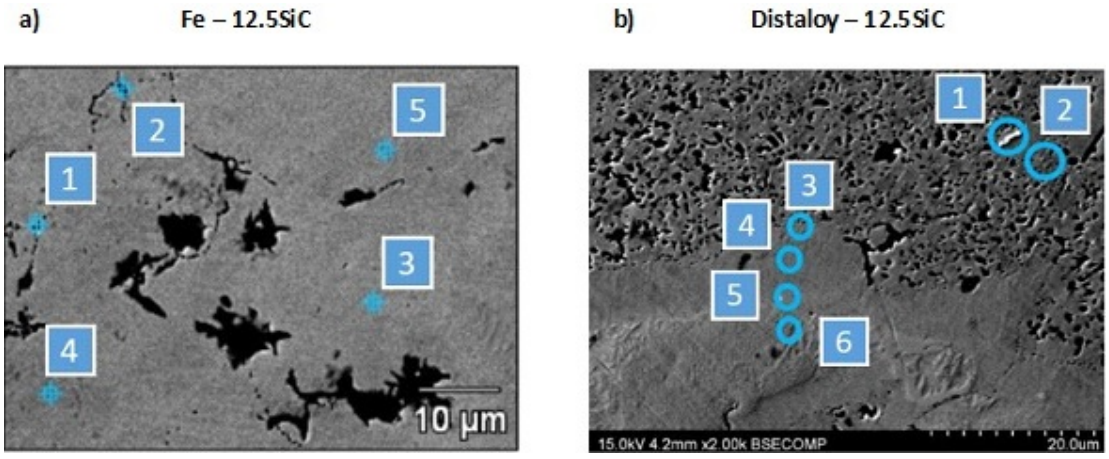

Figure 11. Selected EDS analysis areas for the material a) Fe – 12.5% SiC b) Distaloy SA – 12.5% SiC.

with the composition Distaloy SA – 12.5% SiC (Figure 11b) confirms that in point 1 there is an area of the molybdenum phase located among the agglomerate consisting of dark precipitates, which could have been formed as a result of the decomposition of SiC. Point 2 is located inside the agglomerate and is distinguished by the highest amount of silicon, which is confirmed by the analysis of the chemical composition. The analyzed area where points 3, 4, 5 and 6 were plotted contains respectively decreasing amounts of silicon (Table 4).

The obtained results indicate that for samples based on pure iron, increasing the amount of added silicon carbide does not cause visible changes in hardness. The maximum average hardness value was characterized by samples with the composition Fe – 10% SiC (Figure 12). The remaining samples achieved slightly lower, approximate values. The results of Vickers hardness measurements for materials based on iron Distaloy SA show a similar upward trend as in the case of Fe composites. Hardness rises gradually with increasing the amount of silicon carbide addition and reaches the highest value at a silicon carbide content of 10% (Figure 12). Higher silicon carbide content causes a decrease in the hardness of the tested composites.

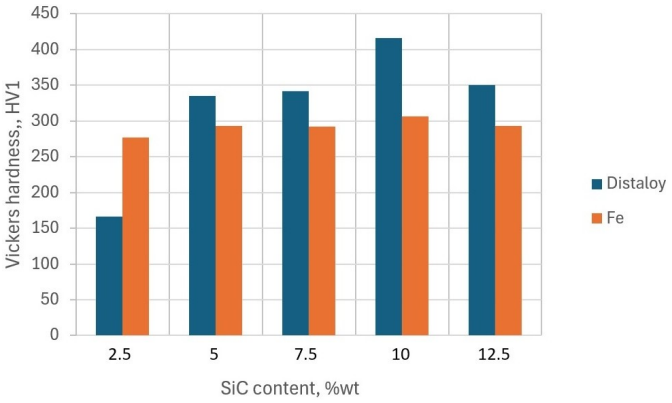

Figure 12. Hardness dependence on SiC content for Fe and Distaloy based composites.

4. CONCLUSIONS

Based on the conducted studies, it can be concluded that the chemical composition of the input material and the grain size have a significant effect on the structure and mechanical properties of the final product. The sintering temperature was selected based on a review of the literature and initial measurements of the density of the obtained samples, the sintering time was determined at 10 minutes. The optimal parameters of the sintering process for Fe–SiC and Distaloy–SiC alloys are: sintering temperature 1000 °C and sintering time 10 min. The highest mechanical properties were achieved for the composite composition containing a SiC additive of 10%. The analysis carried out using scanning microscopy showed that the use of the SPS method in obtaining composite mixtures causes changes in the structures of materials in the form of appearing complex phases. These phases are formed as a result of diffusion, which is activated by the sintering process temperature and has a significant effect on the level of mechanical properties.

It was observed that decomposition of some silicon carbide led to the formation of perlite in samples with 12.5% SiC, in both cases of Fe – 12.5% SiC and Distaloy SA – 12.5% SiC.

REFERENCES

Bedir F., 2007. Characteristic properties of Al-Cu-SiCp and Al-Cu-B4Cp composites produced by hot pressing method under nitrogen atmosphere. *Mater. Des.*, 28, 1238–1244. DOI: 10.1016/j.matdes.2006.01.003.

Chen Y., Song S., Zhu S., Cui X., Zhao F., 2021. Selective laser remelting of in-situ Al_2O_3 particles reinforced AlSi10Mg matrix composite: densification, microstructure and microhardness. *Vacuum*, 191, 110365. DOI: 10.1016/j.vacuum.2021.110365.

Eze A.A., Sadiku E.R., Kupolati W.K., Ndambuki J.M., Snyman J., Ibrahim I.D., 2022. Spark plasma sintering of copper-niobium-graphite composites, and the investigations of their microstructure and properties. *Metals*, 12, 574. DOI: 10.3390/met12040574.

Huang B., Xiong W., Yao Z., Chen S., Zhang M., Yang Q., 2016. Effect of WC content on microstructure and mechanical properties of Ni3Al-bonded cermets. *Ceram. Int.*, 42, 5291–5298. DOI: 10.1016/j.ceramint.2015.12.058.

Jarząbek D.M., Chmielewski M., Wojciechowski T., 2015. The measurement of the adhesion force between ceramic particles and metal matrix in ceramic reinforced-metal matrix composites. *Composites Part A.*, 76, 124–130. DOI: 10.1016/j.compositesa.2015.05.025.

Leszczyńska-Madej B., Garbiec D., Madej M., 2019. Effect of sintering temperature on microstructure and selected properties of spark plasma sintered Al-SiC composites. *Vacuum*, 164, 250–255. DOI: 10.1016/j.vacuum.2019.03.033.

Li P., Gao J., Gong M., Shen D., Tong W., 2020. Effects of manganese on diffusion and wear behavior of ZTA particles reinforced iron matrix composites in vacuum. *Vacuum*, 177, 109408. DOI: 10.1016/j.vacuum.2020.109408.

Madej M., Leszczyńska-Madej B., Garbiec D., 2022. Effect of sintering temperature and iron addition on properties and microstructure of high speed steel based materials produced by spark plasma sintering method. *Materials*, 15, 7607. DOI: 10.3390/ma15217607.

Marnier G., Keller C., Noudem J., Hug E., 2014. Functional properties of a spark plasma sintered ultrafine-grained 316L steel. *Mater. Des.*, 63, 633–640. DOI: 10.1016/j.matdes.2014.06.053.

Muthuchamy A., Annamalai A.R., Karthikeyan M., Thakur A., Nagaraju N., Agrawal D.K., 2018. Microstructural evolution of iron based alloys produced by spark plasma sintering method. *Phys. Met. Metall.*, 119, 678–684. DOI: 10.1134/S0031918X18070062.

Shashanka R., 2019. Non-lubricated dry sliding wear behavior of spark plasma sintered nano-structured stainless steel. *J. Mater. Environ. Sci.*, 10 (8), 767–777.

Sui Y., Zhou M., Jiang Y., 2018. Characterization of interfacial layer of ZTA ceramic particles reinforced iron matrix composites. *J. Alloys Compd.,* 741, 1169–1174. DOI: 10.1016/j.jallcom.2018.01.199.

Sulima I., Kowalik R., Stępień M., Hyjek P., 2024. Effect of ZrB2 content on the properties of copper matrix composite. *Materials*, 17, 6105. DOI: 10.3390/ma17246105.

Wang S., Li Y., Wang J., Zheng Z., Luo T., Zheng K, Long J., 2021. Effect of sintering temperature on the microstructure and properties of Ti/W–C reinforced Fe-based composites. *Vacuum*, 194, 110617. DOI: 10.1016/j.vacuum.2021.110617.

Zalisz Z., Watts A., Mitchell S.C., Wronski A.S., 2005. Friction and wear of lubricated M3 Class 2 sintered high speed steel with and without TiC and MnS additives. *Wear*, 258, 701–711. DOI: 10.1016/j.wear.2004.09.069.

Zapata W.C., da Costa C.E., Torralba J.M., 1998. Wear and thermal behaviour of M2 high speed steel reinforced with NbC composite. *J. Mater. Sci.*, 33, 3219–3225. DOI: 10.1023/A:1004324729342.

Zhang M., Li M., Chi J., Wang S., Ren L., Fang M., Zhou C., 2019. Microstructure evolution, recrystallization and tribological behavior of TiC/WC composite ceramics coating. *Vacuum*, 166, 64–71. DOI: 10.1016/j.vacuum.2019.04.049.

Zhang R., Chen B., Liu F., Sun M., Zhang H., Wu C., 2022. Microstructure and mechanical properties of composites obtained by spark plasma sintering of Ti_3SiC_2-15 vol. %Cu mixtures. *Materials*, 15, 2515. DOI: 10.3390/ma15072515.